Cooling Injection Effect on a Transonic Squealer Tip—Part II: Analysis of Aerothermal Interaction Physics

H. Ma
University of Michigan-Shanghai Jiao Tong University Joint Institute,
Shanghai Jiao Tong University,
Shanghai 200240, China
e-mail: haitengma@gmail.com

Q. Zhang[1]
Department of Mechanical Engineering and Aeronautics,
School of Engineering and Mathematical Sciences,
City, University of London,
Northampton Square,
London EC1V 0HB, UK
e-mail: Qiang.Zhang@city.ac.uk

L. He
Department of Engineering Science,
University of Oxford,
Oxford OX2 0ES, UK
e-mail: Li.He@eng.ox.ac.uk

Z. Wang
University of Michigan-Shanghai Jiao Tong University Joint Institute,
Shanghai Jiao Tong University,
Shanghai 200240, China
e-mail: wangzhaoguang1991@hotmail.com

L. Wang
University of Michigan-Shanghai Jiao Tong University Joint Institute,
Shanghai Jiao Tong University,
Shanghai 200240, China
e-mail: lipo.wang@sjtu.edu.cn

A basic attribute for turbine blade film cooling is that coolant injected should be largely passively convected by the local base flow. However, the effective working of the conventional wisdom may be compromised when the cooling injection strongly interacts with the base flow. Rotor blade tip of a transonic high-pressure (HP) turbine is one of such challenging regions for which basic understanding of the relevant aerothermal behavior as a basis for effective heat transfer/cooling design is lacking. The need to increase our understanding and predictability for high-speed transonic blade tip has been underlined by some recent findings that tip heat transfer characteristics in a transonic flow are qualitatively different from those at a low speed. Although there have been extensive studies previously on squealer blade tip cooling, there have been no published experimental studies under a transonic flow condition. The present study investigates the effect of cooling injection on a transonic squealer tip through a closely combined experimental and computational fluid dynamics (CFD) effort. The experimental and computational results as presented in Part I have consistently revealed some distinctive aerothermal signatures of the strong coolant-base flow interactions. In this paper, as Part II, detailed analyses using the validated CFD solutions are conducted to identify, analyze, and understand the causal links between the aerothermal signatures and the driving flow structures and physical mechanisms. It is shown that the interactions between the coolant injection and the base over-tip leakage (OTL) flow in the squealer tip region are much stronger in the frontal subsonic region than the rear transonic region. The dominant vortical flow structure is a counter-rotating vortex pair (CRVP) associated with each discrete cooling injection. High HTC stripes on the cavity floor are directly linked to the impingement heat transfer augmentation associated with one leg of the CRVP, which is considerably enhanced by the near-floor fluid movement driven by the overall pressure gradient along the camber line (CAM). The strength of the coolant-base flow interaction as signified by the augmented values of the HTC stripes is seen to correlate to the interplay and balance between the OTL flow and the CRVP structure. As such, for the frontal subsonic part of the cavity, there is a prevailing spanwise inward flow initiated by the CRVP, which has profoundly changed the local base flow, leading to high HTC stripes on the cavity floor. On the other hand, for the rear high speed part, the high inertia of the OTL flow dominates; thus, the vortical flow disturbances associated with the CRVP are largely passively convected, leaving clear signatures on the top surface of the suction surface rim. A further interesting side effect of the strong interaction in the frontal subsonic region is that there is considerable net heat flux reduction (NHFR) in an area seemingly unreachable by the injected coolant. The present results have confirmed that this is due to the large reduction in the local HTC as a consequence of the upstream propagated impact of the strong coolant-base flow interactions. [DOI: 10.1115/1.4035200]

1 Introduction

In the development of new-generation gas turbine engines, the turbine inlet temperature keeps increasing to pursue higher efficiency. Advanced cooling technologies are crucial to ensure the survival of turbine blades in the extremely hot environment. Among all the surfaces of the high-pressure (HP) turbine blade, the tip region has the highest thermal load (Bogard and Thole [1]). The primary objective of tip cooling is to reduce surface heat flux with minimal coolant consumption while maintaining the aerodynamic efficiency, and most blade tip cooling are achieved through experience (Bunker [2]).

Most of the tip cooling studies have been conducted at low-speed or high subsonic flow conditions. Thermal performance has been the main focus of these studies. Kwak and Han [3,4] found that higher blowing ratio produces lower heat transfer coefficient (HTC) and higher film cooling effectiveness on the flat and squealer tips. Christophel et al. [5,6] investigated the heat transfer characters of a cooled flat tip experimentally. Better cooling performance was reported for smaller tip gap height. Ahn et al. [7] carried out a parametric study regarding tip geometries, locations of the cooling holes, blowing ratios, and tip clearance. They found that the highest film cooling effectiveness was achieved by injecting coolant from only the pressure side (PS) for the flat tip case and from both the tip and pressure side for the squealer tip case.

[1]Corresponding author.

Contributed by the Structures and Dynamics Committee of ASME for publication in the Journal of Engineering for Gas Turbines and Power. Manuscript received July 14, 2016; final manuscript received August 24, 2016; published online January 10, 2017. Editor: David Wisler.

Similar results were also presented by Mhetras et al. [8]. Newton et al. [9] observed augmented level of heat transfer coefficient surrounding the cooling holes. They attributed this phenomenon to the localized acceleration of the leakage flow between the plumes of the coolant. Similar argument was also presented by Zhou et al. [10]. Krishnababu et al. [11] reported hot spots on the blade tip due to the impingement of the tip leakage flow. High value of cooling effectiveness associated with the coolant entrainment by the squealer cavity flow has been discussed by Mhetras et al. [8], Kwak and Han [3], and Zhou et al. [10].

The alternation of the base OTL aerodynamic pattern has never been the original cooling design intention (Bunker [2]). However, there are several studies which reported effective blockage effect due to cooling injection, such as Niu and Zang [12], Krishnababu et al. [11], Naik et al. [13], Couch et al. [14], and Hohlfeld et al. [15]. Experimental study by Newton et al. [9] indicates that cooling injection into the tip gap makes the leakage vortex smaller and weaker and can eliminate the separation bubble present in the uncooled case.

Effective cooling strategy should first begin with a good knowledge of the base OTL flow. The transonic nature of HP turbine blade tip and qualitative different tip heat transfer behavior has been revealed by recent studies (Zhang et al. [16,17], Wheeler et al. [18], O'Dowd et al. [19] and Zhang and He [20]). Li et al. [21] reported that the transonic squealer tip leakage flow is not sensitive to the cavity depth due to its choking nature, which also contradicts the previous findings in low speed condition.

Wang et al. [22] investigated the detailed flow physics between coolant and tip leakage flow on an idealized transonic tip model. They found the formation of a counter-rotating vortex pair, which redistributes the leakage mass flow rate locally. Due to flow choking and sensitivity of transonic OTL flow on cooling injection, the aerodynamic design ranking of squealer tip over flat tip has been reversed. Similar finding has also been reported by Hofer and coworkers [13] and Wheeler and Saleh [23].

Therefore, an efficient tip cooling design has to be determined by an iterative aero-thermal optimization process. In practice, further complication could also be introduced by the coupling of heat transfer and aerodynamics under the engine condition temperature ratio (Maffulli and He [24,25], Zhang and He [26]).

The aero-thermal interaction physics of transonic squealer tip cooling has not been well understood. Most of the related CFD analysis is lack of experimental validation. This two-part paper series aims to investigate the effect of cooling injection on a transonic squealer tip through a closely combined experimental and CFD effort. The first of the kind of experimental data on the squealer tip cooling under transonic conditions are reported in Part I (Ma et al. [27]). A series of cooling holes were placed with different location and spacing. Validated by the experimental heat transfer data, the CFD analysis in this Part II paper aims to address the complex interaction mechanism between cooling injection and OTL flow. The driving aerodynamic mechanisms behind the non-intuitive heat transfer signatures reported in the experimental study, and more importantly, its implication on tip cooling design strategy, will be discussed.

2 Method

As introduced in Part II (Ma et al. [27]), ANSYS Fluent is employed in the present study for numerical simulations. Two Reynolds-averaged Navier–stokes (RANS) models, Spalart–Allmaras model (SA) and k–ω shear stress transport (SST) model (SST), are implemented and validated against experimental data. The computational domain is a single blade passage with periodic boundary condition, as shown in Fig. 1. For the coolant supply system, only the feed pipes above the plenum inside the upper blade are modeled. The geometric dimensions, such as the tip gap height, the configuration of cooling holes including the feed pipe length, the blade profile, are exactly the same as the experimental setup described in Part II of the paper.

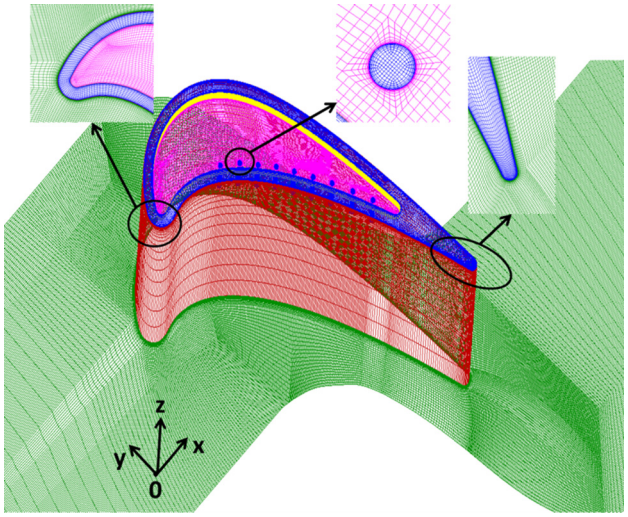

Fig. 1 Computational domain and mesh employed in the present study

The total pressure and total temperature at the cascade inlet and the inlet of coolant feed pipes, as well as the static pressure at the cascade outlet, are also set the same as the experimental study ($P_{0,i} = 180$ kPa, $T_{0,i} = 300$ K, $P_{0,c} = 198$ kPa, $T_{0,c} = 270$ K, $P_{s,e} = 101$ kPa). Because the main focus of the simulation is on tip heat transfer, the boundary condition on the hub is set to be symmetric to reduce the computational cost. The effect of hub endwall secondary flow on tip leakage flow is considered negligible. No-slip boundary conditions are imposed on all the solid walls.

Isothermal boundary conditions with two different temperatures (250 K and 260 K) are set on all the walls. The wall heat flux from these two cases is subtracted to calculate heat transfer coefficient. The assumption here is that heat transfer coefficient only depends on aerodynamics and is independent of the thermal boundary conditions, which is reasonable when the temperature change is small.

Structured mesh with a grid size of 5×10^6 was generated by using Pointwise software. The maximum included angle is controlled within 140 deg. Smooth transitioning is guaranteed at the interface between different mesh blocks. The five-hole case uses the same mesh as the nine-hole case, with additional holes being blocked during numerical computation.

Detailed mesh sensitivity study has been carried out for both Spalart–Allmaras model (SA) and k–ω SST model (SST). The averaged results are listed in Table 1. For all the cases, average y^+ value on tip surfaces is around one to resolve the near-wall boundary layer. The predicted average value of HTC and adiabatic temperature have relatively large change when the number of grid points across the tip gap is increased from 18 to 30, but their change is only marginal when the tip gap points are further increased to 42. Figure 2 shows spatially resolved results of the relative difference in HTC between different grid sizes. Generally,

Table 1 Mesh and turbulence model dependence studies

Grid size		3×10^6	5×10^6	7×10^6
Grid points within tip gap		18	30	42
Average y^+ on tip surfaces	SA	0.826	0.824	0.823
	SST	0.867	0.883	0.886
Average HTC (W/(m^2 K))	EXP	1199.1		
	SA	1120.5	1102.7	1097.6
	SST	1200.8	1273.8	1301.1
Average $T_{ad}/T_{0,i}$	EXP	0.9800		
	SA	0.9889	0.9887	0.9887
	SST	0.9912	0.9901	0.9903

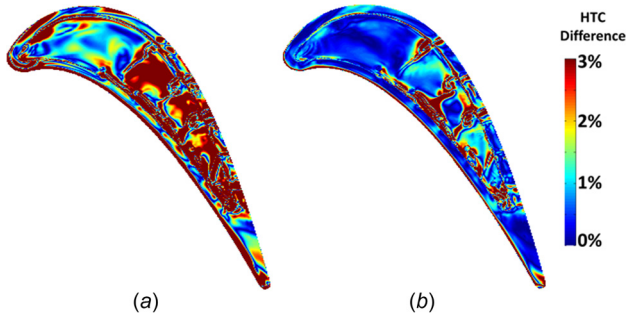

Fig. 2 Contours of the relative difference in HTC between the results from two meshes for the cooled case (five cooling holes near the PS side)

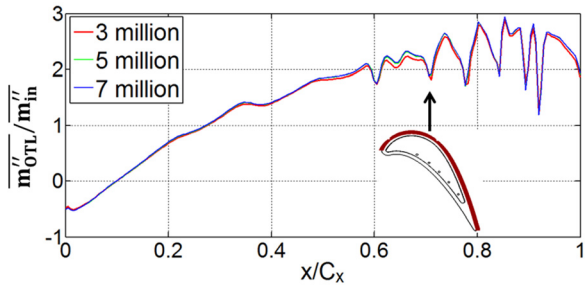

Fig. 3 Nondimensional radially averaged OTL mass flux distribution on the suction side edge of the squealer tip for the cooled case (five cooling holes near the PS side)

the local HTC difference between 5 and 7×10^6 cells is less than one percent for the majority of the tip surface (except some area near the cooling holes). Figure 3 presents the nondimensional radially averaged OTL mass flux over the suction side (SS) rim. Grids with 5×10^6 to 7×10^6 sizes show same local distribution of leakage flow along the blade. Therefore, the 5×10^6 mesh is considered adequate for the computations discussed later.

3 Results and Discussion

The present computational analyses are based on the CFD solutions with Spalart–Allmaras model (SA), which have been validated in Part II (Ma et al. [27]). We will first examine the overall cooling-base flow interactions and the impacts on both the basic flow patterns and aerothermal performance parameters. We will then establish the key driving vortical flow structure and physical mechanisms for a discrete cooling hole. Finally, the interplay and balance of the interplay among the holes and between the coolant and base flow will be used to explain the distinctive aerothermal patterns and variations as experimentally and computationally observed.

3.1 Overall Aerothermal Impact of Coolant Injection. For convective heat transfer, HTC is dominated and driven by aerodynamics. So, a change in HTC should be an indicator of the change in aerodynamics. In other words, the change in HTC should be a measure of the effective relevant change in aerodynamics as far as the convective heat transfer is concerned.

Figure 4 shows both experimental and CFD results of HTC contours for three cases (two cooled configurations compared to the uncooled tip). Distinctly high HTC stripes are clearly identified for all the cooling cases. Some previous results (Zhou [28], Newton et al. [9,29], Christophel et al. [6]) reported as well that cooling injection could enhance local HTC values near the cooling holes, mostly. However, such high HTC stripes as observed in the present results have not been reported before. Since the cooling effectiveness as reported in Part I of the paper tends to be small for the cases considered, the marked rise in HTC values in

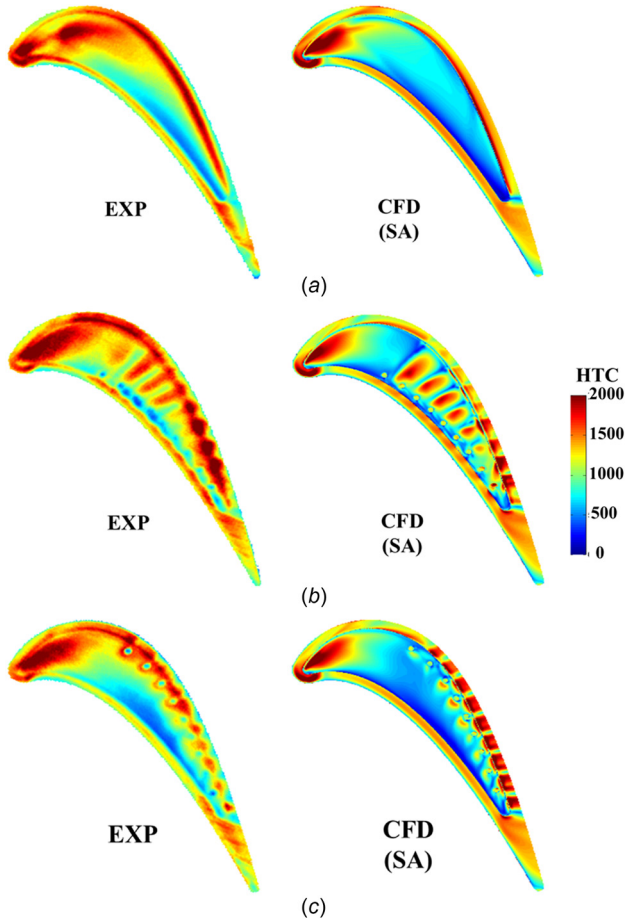

Fig. 4 Comparison of HTC (W/(m^2-K))

these stripes would imply corresponding additional undesirable hot spots to be dealt with.

Percentage differences in HTC ($(HTC_{cooled} - HTC_{uncooled})/HTC_{uncooled}$) between the two cooled cases and the uncooled case are plotted in Fig. 5. Both the experimental and CFD results

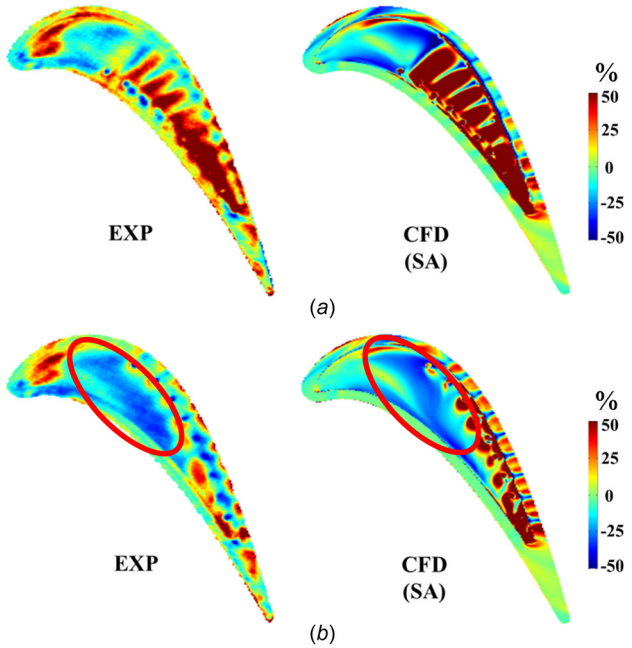

Fig. 5 Percentage differences in HTC (all relative to the uncooled case)

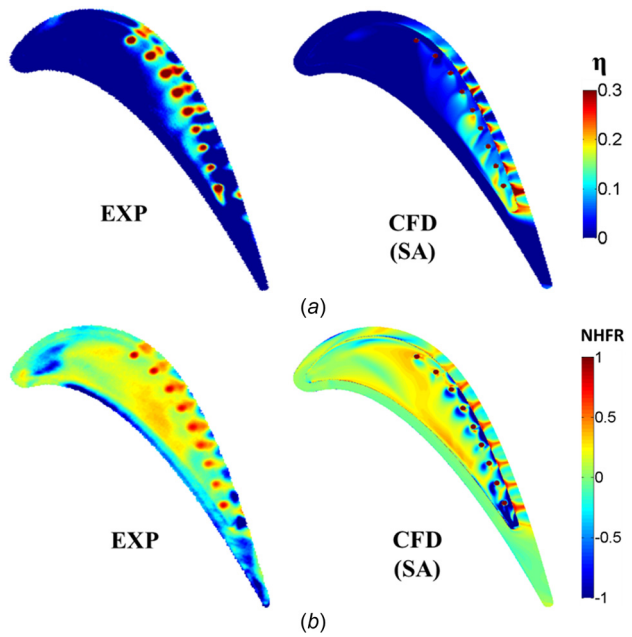

Fig. 6 Cooling parameters (case with nine holes near SS)

consistently show that in the striped region near the cooling holes, HTC value increases by over 50%.

Interestingly, even far away from the cooling holes, HTC can be decreased by over 20%. Particular attention is drawn to the large frontal part of the cavity floor for case with cooling holes near the suction surface rim (Fig. 5(*b*)). There is a large change in the local HTC in the area, which is not expected to be reached by the coolant.

To elaborate this further, corresponding plots of the cooling effectiveness and the net heat flux reduction (NHFR) are given in Fig. 6. Clearly, the coolant film has hardly meaningful signature in the cavity floor area of interest (Fig. 6(*a*)). So, clearly the coolant cannot reach the area of the interest. Therefore, the change in the HTC in this area is the indicator of the aerodynamic changes due to the upstream propagated influence of the coolant injection. Indeed, in this area, the HTC has been significantly reduced via the propagated impact by the coolant injection, for which the corresponding change of flow field will be illustrated later. And it is the change of the HTC (rather than cooling effectiveness) that has led to the significant change of the net heat flux reduction in the corresponding area (Fig. 6(*b*)).

Figure 7 illustrates the overall flow patterns over the tips. Streamlines are colored by the Mach number contours. First, it is noted that for both the cooled and uncooled cases, flow choking does exist over the suction side rim for the rear part of the blade tip. There seems to be a clear overall contrast between the frontal part and rear part when the cooling is introduced. The flow in the frontal part (completely subsonic) seems to be much more influenced by the injection. The rear one is far less changed by the injection; in particular, the streamlines of the over-tip-leakage flow near the trailing edge remain more or less unaffected.

Regarding the impact of cooling injection, we clearly see that the coolant from each cooling hole is separated into two branches after injection. The cavity flow is interrupted by the coolant.

To examine the OTL mass flux quantitatively, a nondimensional radially averaged OTL mass flux is defined on the squealer edges as

$$\frac{\overline{m''_{\mathrm{OTL}}}}{\overline{m''_i}} = \frac{\left[\int_0^g (\rho \mathbf{V}\cdot\mathbf{n})\ dz\right]\Big/ g}{\left[\int (\rho \mathbf{V}\cdot\mathbf{n})\ dl\right]\Big/ l} \tag{1}$$

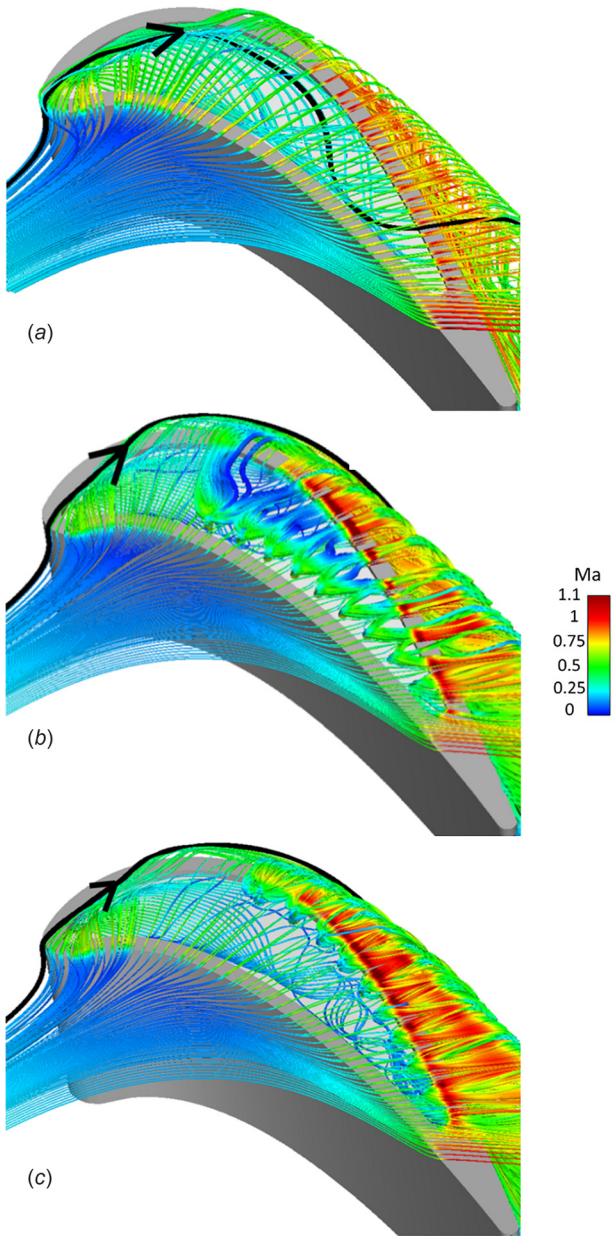

Fig. 7 OTL flow streamlines for uncooled and cooled cases

where g is the tip gap height (%1 of blade span), l represents a line at the midspan of the cascade inlet.

Figure 8 plots the distribution along the axial chord for such nondimensional radially averaged OTL mass flux. Overall, the

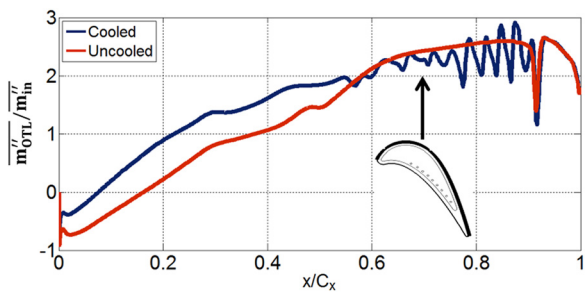

Fig. 8 Nondimensional radially averaged OTL mass flux distribution on the suction side edge of squealer tip

Table 2 Over-tip leakage mass flow rate and loss

	PS9	CAM9	SS9
$\frac{\dot{m}_{OTL}}{\dot{m}_m}$	0.028		
$\frac{\dot{m}_c}{\dot{m}_{OTL-uc}}$	0.164	0.163	0.161
$\frac{\dot{m}_{OTL-PS}}{\dot{m}_{OTL-uc}}$	0.899	0.903	0.916
ζ	0.140	0.140	0.141

leakage mass flux results shown in Fig. 8 are in line with the basic observation that the frontal part is more influenced by the cooling injection than the rear part. On the SS edge, OTL mass flux increases near the leading edge after cooling injection. This is in line with the change of the OTL flow pattern as illustrated in Fig. 7. In the midchord (60–90%) region, a wavy behavior is exhibited in the OTL mass flux, corresponding to the coolant injected from discrete holes. This seems to indicate that the discreet behavior of each cooling hole is manifested more strongly toward downstream. However, near the trailing edge, the OTL mass flux is not changed at all by the cooling injection. This suggests that coolant cannot reach this area.

Table 2 lists the nondimensional mass flow rates and loss coefficient (defined same as Want et al. [22]) for various cases considered. The ratio between the span (S) and the axial chord (C_x) is 1.8. The tip gap height (g) is 1% of span. The overall averaged leakage flow is 2.8% of the main stream one ($\dot{m}_m$). All the leakage flow for cooled cases is normalized by that of the uncooled one. It can be seen that the leakage entering the pressure side rim ($\dot{m}_{OTL-PS}$) is about 10% smaller than that of the uncooled case ($\dot{m}_{OTL-uc}$) due to the blockage of the cooling injection. Note that the amount of the coolant is relative small (about 16% of the over leakage mass flow for the uncooled case) and remains largely unchanged for the three cooled cases. The overall strong impact of the small amount of cooling is rather remarkable.

3.2 Driving Vortical Flow Structure and Impact. In the following analysis, we look more closely at the case with nine cooling holes near pressure surface rim, as this case seems to have the largest changes in the overall flow pattern (Fig. 7(*b*)) as well as the clearest high HTC stripes of interest (Fig. 4(*b*)).

The average level of blowing ratio is 1.2, with reference to the mass-averaged flow state of the OTL over the PS edge. For the nine cooling holes, the local blowing ratio deviates within ±2%, and thus, the blowing coolant ejection is roughly regarded as constant for all holes. Similar results on the variation of local blowing ratio were also reported by Zhou [28].

The flow topology of the injection is illustrated in Fig. 9(*a*). The injected coolant first hits the casing and then bifurcates. We also use a nondimensional total temperature θ to identify the relative influence of the coolant and the OTL flow in the highly mixed region. The definition of θ is

$$\theta = \frac{T_{0,i} - T_0}{T_{0,i} - T_c} \tag{2}$$

where $T_{0,i}$ is the inlet mainstream total temperature, T_c is the coolant temperature, and T_0 is the local total temperature. Clearly, θ close to one means coolant-dominant (cool), while θ near zero is OTL flow dominant (hot). Figure 9(*b*) gives the contours of θ on plane N, which is cut normal to the camber line. It is clearly shown that the coolant impinges on the casing directly after injection. The OTL flow is locally blocked by the coolant and has to bypass the coolant core afterwards.

To resolve the vorticity in the three-dimensional tip flow field onto a two-dimensional plane, a normal vorticity (ω_n) is defined

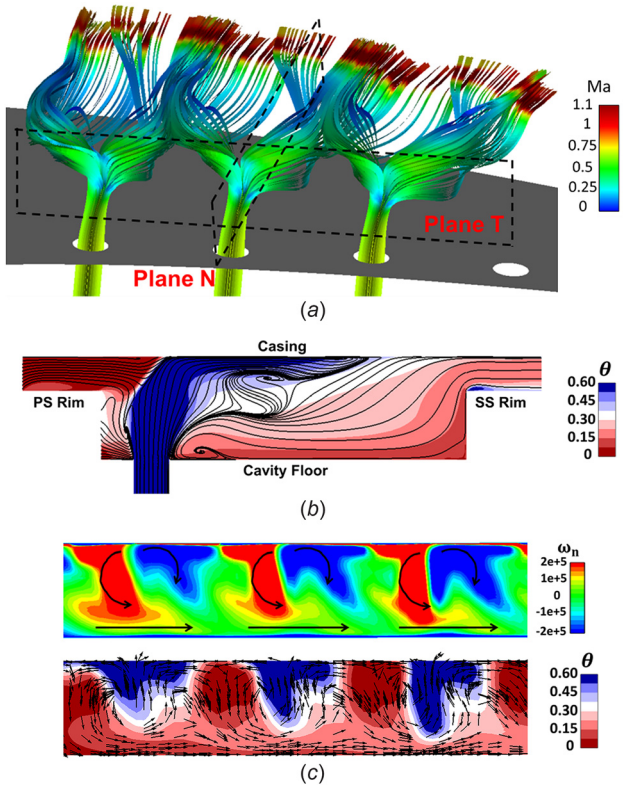

Fig. 9 Injection vortical flow structure

as the dot product of vorticity and the normal vector of the plane. Physically, the normal vorticity represents the rotation of the flow as projected on that plane, with counter-clockwise direction designated as a positive rotation.

Figure 9(*c*) shows the contours of ω_n together with θ on plane T, which is cut tangentially to the camber line downstream of the cooling holes (as shown in Fig. 9(*a*)). From the contours of normal vorticity, a counter-rotating vortex pair (CRVP) is clearly observed downstream of each cooling hole. The location of the CRVP is near the casing. The CRVP is formed by the coolant jet in the OTL flow. It is in line with the basic fluid mechanics researches about jets in crossflow (Cortelezzi and Karagozian [30], Smith and Mungal [31]). The existence of the CRVP in the blade tip cooling has also been computationally demonstrated by Wang et al. [22] using an idealized quasi-3D tip cooling model. It is pointed out, however, in the present case, that the two legs of the CRVP are not symmetrical. The left leg (red) is shown to be considerably stronger than the right leg (blue), as shown in Fig. 9(*c*). Interactions between CRVPs from neighboring cooling holes also exist. The right leg of one CRVP meets the left leg of the adjacent CRVP, and their combined effect should be pressing the flow between them downward to the cavity floor.

From Fig. 9(*c*), we can also see that coolant is concentrated in a small region near the casing on plane T (blue). The two-dimensional velocity vector shows that in the middle of each coolant-concentrated region, the flow moves straightly upward and impinges on the casing. To the left and right of the impingement line, the flow has opposite directions of rotation, corresponding to two branches of the coolant shown in Fig. 9(*a*). The region between each coolant is occupied by the OTL flow (red). In this OTL-concentrated region, the hot OTL flow is strongly entrained by the left leg of the CRVP on the right side and the right leg of the CRVP on left. Consequently, the entrained hot OTL flow in this region has a strong spanwise inward component to move to the cavity floor.

Combining the two contours in Fig. 9(*c*), we can already establish that the downward motion in the OTL-concentrated region is

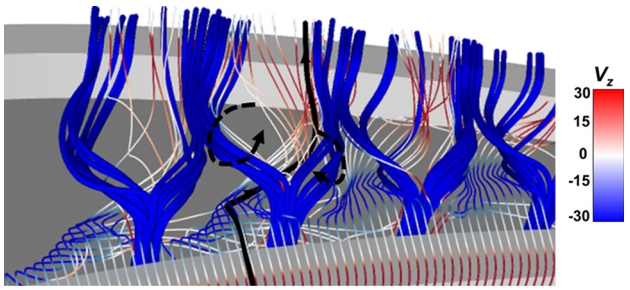

Fig. 10 Streamlines of OTL flow (colored by radial velocity) and the injected coolant (blue) (black line indicates the OTL flow path)

caused by the interaction between two adjacent CRVPs. The two-dimensional velocity vectors also show clearly that near cavity floor beneath the CRVPs, there is a net fluid movement along camber line from leading edge to the trailing edge (Fig. 9(*c*)). This chordwise movement is believed to be caused by the overall chordwise pressure gradient in the cavity (i.e., higher pressure near leading edge and lower pressure near trailing edge). The hot fluid near cavity floor, entrained by the coolant CRVPs, will have little inertia, and thus, is very amenable to the overall pressure gradient. The resultant chordwise movement of the near-wall fluid will consequently enhance the left anti-clockwise leg and depress the right clockwise leg, leading to the no symmetry of the two legs of a CRVP, as observed.

Having established the influencing behavior of the driving CRVP vortical structure, we now use Fig. 10 to underline the OTL flow as the influenced part. Figure 10 shows the flow patterns of the OTL flow together with the injected coolant. This figure is provided to illustrate how the OTL flow is influenced by the spanwise entrainment of the CRVP vortical flow by the cooling injection. So, the OTL flow streamlines are colored by the spanwise velocity (V_z). Right after entering the tip gap over the PS rim, the OTL flow has little or no spanwise velocity component. For an uncooled case (Fig. 7(*a*)), the OTL flow will remain largely flowing straight over the cavity flow without much interaction with the flow inside the cavity. This is no longer the case once the cooling injection is introduced (Fig. 10); the OTL flow after entering the cavity region clearly dives into the cavity with considerable inward spanwise velocity (negative V_z). This is caused by the pressing force between the right leg of one CRVP and the left leg of the adjacent CRVP. The OTL flow then goes beneath the injected coolant and moves toward trailing edge, driven by the overall chordwise pressure gradient discussed earlier. It acts as an enhancement to the left leg of the CRVP as it rotates in the same direction with this stronger leg, before exiting the tip gap over the SS rim.

The impact of cooling injection on the cavity flow can also be indicated from a different perspective as shown in Fig. 11. Figure 11 shows the contours of radial velocity on the cut plane of the rim surface for the cooled and uncooled cases. Superimposed are the streamlines on these planes. For the nine holes near the pressure side (Fig. 11(*b*)), we see considerable negative radial velocities in striped regions, where OTL flow plunges into the cavity floor. Toward the trailing edge, the diving of OTL flow is weaker. For the uncooled case, radial velocity for most area is quite small.

The flow pattern on two selected cut planes is also shown in Fig. 11. For the nine holes near the pressure side, OTL flow near the midchord is pressed down and impinges on the cavity floor. In contrast, the OTL flow near the trailing edge tends to pass over the cavity directly. Compared with the uncooled case, the OTL flow pattern is greatly changed by the cooling injection in the frontal and midchord regions, whereas it stays largely the same near the trailing edge. Similar observations have also been

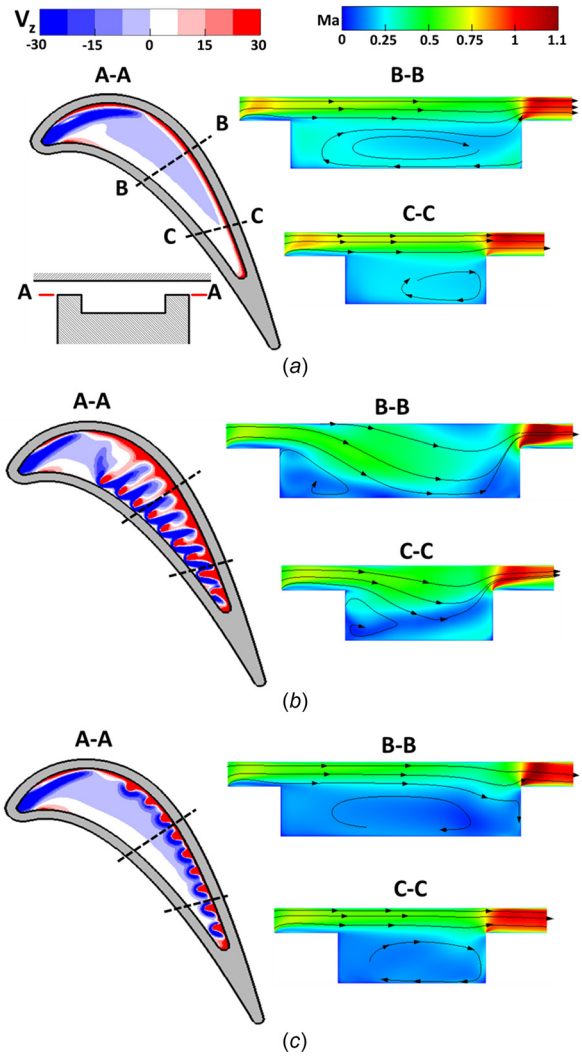

Fig. 11 Contours of radial velocity on the cut plane of the rim surface (A–A) and contours of Mach number on two cut planes normal to the camber line (B–B and C–C)

reported by Kwak and Han [3] and Mhetras et al. [8], though mainly for low speed flows.

Figure 11(*c*) also indicates that there is a considerable reduction of cavity flow velocity (Mach number) even for the regions clearly unreachable by the coolant injected. This reinforces the interpretation that the cooling injection can have considerable upstream propagated impact on the base flow. In this case, the corresponding changes in HTC can have marked impact on the net heat flux reduction (Fig. 5(*b*)).

3.3 Heat Transfer Signature and Overall Trend. The analyses so far have established the driving vortical flow mechanisms due to the coolant injection, and the responding behavior of the OTL flow. The thermal field characteristics can now be more easily analyzed and understood.

Figure 12 illustrates the contours of nondimensional temperature on plane T2 (tangential to the camber line) and the HTC contours on the cavity floor. From the θ contours, the separation between the coolant and the OTL dominated regions is observed in the radial direction. The coolant is concentrated near the casing, while the OTL flow is mostly entrained inward and located near the cavity floor. This explains the low values of cooling effectiveness on the cavity floor as shown in Fig. 15 in Part I (Ma et al. [27]).

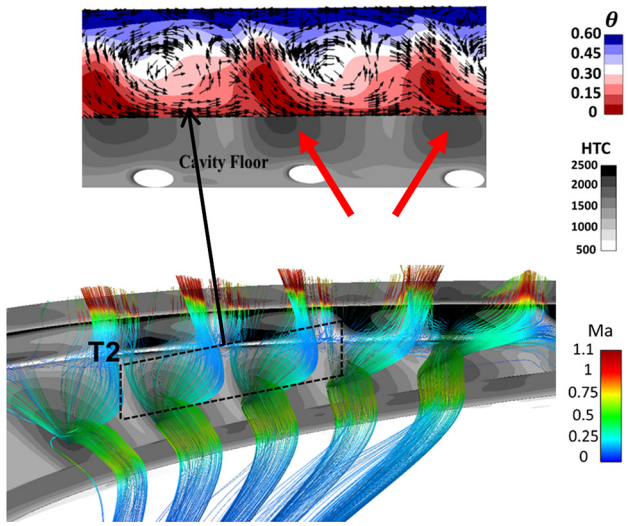

Fig. 12 Contour of nondimensional total temperature on plane T2 and contour of HTC on tip surfaces, with streamlines of OTL flow colored by Mach number (the high HTC regions on the cavity floor are marked by two arrows)

The central point arisen from inspecting Fig. 12 is that the high HTC stripe on the cavity floor is predominantly caused by the flow impingement, and the impinging fluid is mainly originated from the OTL flow. More specifically, Fig. 12 shows the streamlines emitted from the hot OTL fluid regions with $\theta < 0.2$.

The strong left leg of the unsymmetrical CRVP as enhanced by the chordwise fluid movement near cavity flow is only expected to help strengthen the impingement. As such, we have the distinctive HTC stripes as observed.

We now turn our attention to the overall trend of the variation of the high HTC stripes. From Fig. 4(*b*), we notice that the HTC stripes on the cavity floor seem to reduce their strength from the frontal part to the rear part. However, an opposite trend seems to exist for the stripes on the top surface of the suction side rim. We now examine these opposing trends by looking at the variations of the dominant vortical flow structure along the chord.

Figure 13 shows the flow pattern variation along the curved surface cuts on the cavity floor and on the SS rim. The positions of the two curved cut planes are indicated in Fig. 13(*a*). The normal vorticity and the nondimensional total temperature contours on the cut plane over the cavity floor are plotted in Fig. 13(*b*), and those on the curved cut surface over the suction surface rim are shown in Fig. 13(*c*).

Comparing Figs. 13(*b*) and 13(*c*), we can see that moving from a midchord region to the trailing edge, the vortical flow structures are radially moving outward from cavity floor to casing inside the cavity. But on the other hand, those vortical flow patterns over the SS rim are moving inwardly from the casing to the rim top surface. A likely explanation for these contrasting trends over the cavity and over SS rim is to do with the overall changed balance between the base OTL flow and the cooling injection.

The relatively low momentum of the OTL in the frontal part (due to the relatively low local driving pressure difference across the tip) means that OTL can be more easily altered significantly as we have observed.

Toward the trailing edge, the baseline OTL flow has considerably higher momentum. So, the balance between the OTL and the cooling injection has been changed significantly to favor the base OTL flow. As a result, the local coolant flow becomes far less active and more passively convected. The basic CRVP structure as a result of the cooling flow turning and bifurcation remains more or less the same, but its impact is no longer as profound as it has for the frontal part.

In line with the above considerations, the vorticity values for the far upstream region of strong interactions are relatively low, indicating low vorticity residual left once the flow reaches the suction surface rim. On the other hand, the much stronger vorticities toward the downstream regions indicate a weak local interaction, which is again consistent with the interpretation that the local cooling-related vortical structures are largely passively convected by the local base OTL flow.

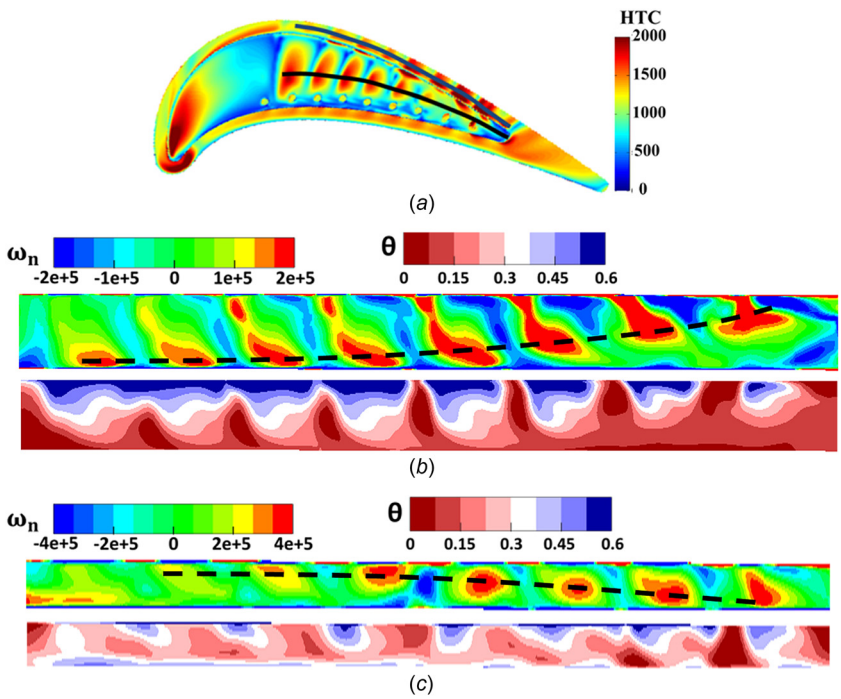

Fig. 13 HTC, vorticity, and temperature variations along two curved surface cuts on the cavity floor and on the SS rim

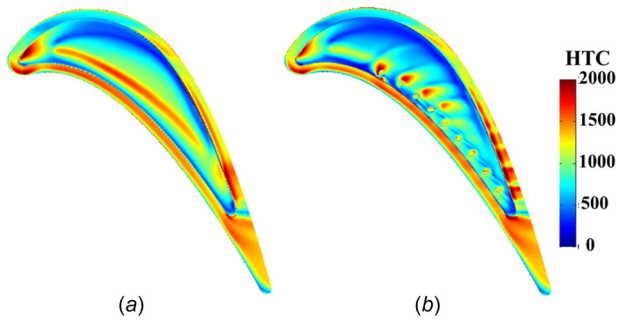

Fig. 14 HTC with relative casing movement (CFD) (W/(m^2-K))

3.4 Further Discussions on Relative Casing Movement Effect. It has been recognized that the relative casing movement could affect the detailed near-tip aerothermal field considerably. In the present study, numerical simulations were also carried out by imposing an anti-rotating motion on the outer casing wall (translation speed of 230 m/s). Figure 14 shows the contours of HTC with relative casing motion. For the uncooled case shown in Fig. 14(*a*), a long region of high heat transfer is formed within the cavity, which is consistent with previous numerical simulation by Virdi et al. [32]. For the cooled case, Fig. 14(*b*) illustrates distinctive thermal stripes on both the cavity floor and the SS rim surface, which are very similar to the trends discussed in the previous stationary cases. Clearly, observations and fundamental understandings obtained in the stationary cases remain valuable and important to the rotating application.

So far, we are still not in the position to further investigate the relative casing motion effect without the support of experimental data.

4 Conclusions

The present study is motivated by the need to enhance fundamental understanding of cooling-base flow interaction for a transonic turbine rotor blade tip in general, and the lack of experimental data for transonic squealer tips in particular. To this end, a combined experimental and CFD investigation has been carried out. In Part I, the first of the kind experimental heat transfer data for a transonic squealer with tip injection are presented. Both the experimental and computational results have shown distinctive aerothermal features which potentially can have marked impact on aerothermal performance of a cooled blade tip.

In this paper, as Part II, detailed analyses based on the validated CFD solutions are presented to identify, analyze, and understand the causal links between the aerothermal signatures and driving flow physical mechanisms. The main findings are as follows.

It is found that cooling injection significantly changes the overall aerodynamics in the tip region. HTC values are altered by over 50%. It is noted that the interactions between the coolant injection and the base over-tip-leakage (OTL) flow are much stronger in the frontal subsonic region than in the rear transonic region.

The dominant driving flow structure is a counter-rotating vortex pair (CRVP) associated with each discrete cooling hole. This is primarily caused by the bifurcation of coolant impinging on the casing. High HTC stripes on the cavity floor are directly linked to the impingement heat transfer augmentation associated with one leg of the CRVP, which has been markedly enhanced by the near-floor fluid movement driven by the overall pressure gradient along the camber line.

The strength of the coolant-base flow interaction as signified by the augmented values of the HTC stripes is seen to correlate to the interplay and balance between the OTL flow and the cooling CRVP. As such, for the frontal subsonic part of the cavity, there is a prevailing spanwise inward flow initiated by the CRVP, which has profoundly changed the local base OTL flow, leading to strong HTC stripes on the cavity floor. On the other hand, for the rear high speed part, the high inertia of the OTL flow dominates; thus, the vortical flow disturbances associated with the CRVP are largely passively convected, only leaving signatures on the top surface of the suction side rim.

Another interesting consequence of the strong cooling-base flow interactions in the frontal cavity region is that there is considerable net heat flux reduction in an area seemingly unreachable by the injected coolant. The present results have confirmed that this is due to the large reduction in the local HTC (with almost no contribution in terms of film cooling effectiveness) as a consequence of the upstream propagated impact of the strong coolant-base flow interaction.

Additionally, it is worth noting that the high HTC stripes due to the flow impingement are largely associated with the OTL flow, instead of the coolant. These high HTC stripe areas are therefore potential hot spots, and thus their implications need to be duly considered in tip cooling designs.

Acknowledgment

The authors gratefully acknowledge the support of Chinese National Science Foundation (51376127) for funding this work.

Nomenclature

C_x = axial chord (m)
CAM = camber line
CRVP = counter-rotating vortex pair
g = tip gap height (m)
HP = high-pressure
HTC, h = heat transfer coefficient (W/(m^2-K))
l = line at the midspan of the cascade inlet
$\dot{m}$ = mass flow rate (kg/s)
m$''$ = mass flux (kg/m^2)
NHFR = net heat flux reduction
OTL = over-tip-leakage
PS = pressure side
S = span (m)
SS = suction side
T = temperature (K)
V = velocity (m/s)

Subscripts

ad = adiabatic
c = coolant, cooled
e = exit of linear cascade
i = inlet of linear cascade
m = mainstream
s = static
uc = uncooled
z = spanwise direction
0 = total

Greek Symbols

ζ = loss coefficient
η = cooling effectiveness
θ = nondimensional total temperature
ρ = density (kg/m^3)
ω_n = normal vorticity (s^{-1})

References

[1] Bogard, D. G., and Thole, K. A., 2006, "Gas Turbine Film Cooling," J. Propul. Power, **22**(2), pp. 249–270.
[2] Bunker, R. S., 2006, "Axial Turbine Blade Tips: Function, Design, and Durability," J. Propul. Power, **22**(2), pp. 271–285.

[3] Kwak, J. S., and Han, J. C., 2003, "Heat Transfer Coefficients and Film Cooling Effectiveness on the Squealer Tip of a Gas Turbine Blade," ASME J. Turbomach., **125**(4), pp. 648–657.
[4] Kwak, J. S., and Han, J. C., 2003, "Heat Transfer Coefficients and Film-Cooling Effectiveness on a Gas Turbine Blade Tip," ASME J. Heat Transfer, **125**(3), pp. 494–502.
[5] Christophel, J. R., and Thole, K. A., 2005, "Cooling the Tip of a Turbine Blade Using Pressure Side Holes—Part I: Adiabatic Effectiveness Measurements," ASME J. Turbomach., **127**(2), pp. 270–277.
[6] Christophel, J. R., Thole, K. A., and Cunha, F. J., 2005, "Cooling the Tip of a Turbine Blade Using Pressure Side Holes—Part II: Heat Transfer Measurements," ASME J. Turbomach., **127**(2), pp. 278–286.
[7] Ahn, J., Mhetras, S., and Han, J.-C., 2005, "Film-Cooling Effectiveness on a Gas Turbine Blade Tip Using Pressure-Sensitive Paint," ASME J. Heat Transfer, **127**(5), pp. 521–530.
[8] Mhetras, S., Yang, H., Gao, Z., and Han, J.-C., 2006, "Film-Cooling Effectiveness on Squealer Cavity and Rim Walls of Gas-Turbine Blade Tip," J. Propul. Power, **22**(4), pp. 889–899.
[9] Newton, P., Lock, G. D., Krishnababu, S., Hodson, H., Dawes, W., Hannis, J., and Whitney, C., 2009, "Aerothermal Investigations of Tip Leakage Flow in Axial Flow Turbines—Part III: Tip Cooling," ASME J. Turbomach., **131**(1), p. 011008.
[10] Zhou, C., Hodson, H., and Lock, G., 2012, "Thermal Performance of Different Cooled Tips in a High-Pressure Turbine Cascade," J. Propul. Power, **28**(5), pp. 900–911.
[11] Krishnababu, S. K., Hodson, H. P., Booth, G. D., Lock, G. D., and Dawes, W. N., 2010, "Aerothermal Investigation of Tip Leakage Flow in a Film Cooled Industrial Turbine Rotor," ASME J. Turbomach., **132**(2), p. 021016.
[12] Niu, M., and Zang, S., 2011, "Experimental and Numerical Investigations of Tip Injection on Tip Clearance Flow in an Axial Turbine Cascade," Exp. Therm. Fluid Sci., **35**(6), pp. 1214–1222.
[13] Naik, S., Georgakis, C., Hofer, T., and Lengani, D., 2012, "Heat Transfer and Film Cooling of Blade Tips and Endwalls," ASME J. Turbomach., **134**(4), p. 041004.
[14] Couch, E., Christophel, J., Hohlfeld, E., Thole, K. A., and Cunha, F. J., 2005, "Comparison of Measurements and Predictions for Blowing From a Turbine Blade Tip," J. Propul. Power, **21**(2), pp. 335–343.
[15] Hohlfeld, E. M., Christophel, J. R., Couch, E. L., and Thole, K. A., 2005, "Predictions of Cooling From Dirt Purge Holes Along the Tip of a Turbine Blade," Int. J. Turbo Jet-Engines, **22**(3), pp. 139–152.
[16] Zhang, Q., He, L., Wheeler, A., Ligrani, P., and Cheong, B., 2011, "Overtip Shock Wave Structure and Its Impact on Turbine Blade Tip Heat Transfer," ASME J. Turbomach., **133**(4), p. 041001.
[17] Zhang, Q., O'Dowd, D., He, L., Oldfield, M., and Ligrani, P., 2011, "Transonic Turbine Blade Tip Aerothermal Performance With Different Tip Gaps—Part I: Tip Heat Transfer," ASME J. Turbomach., **133**(4), p. 041027.
[18] Wheeler, A. P., Atkins, N. R., and He, L., 2011, "Turbine Blade Tip Heat Transfer in Low Speed and High Speed Flows," ASME J. Turbomach., **133**(4), p. 041025.
[19] O'Dowd, D., Zhang, Q., He, L., Oldfield, M., Ligrani, P., Cheong, B., and Tibbott, I., 2011, "Aerothermal Performance of a Winglet at Engine Representative Mach and Reynolds Numbers," ASME J. Turbomach., **133**(4), p. 041026.
[20] Zhang, Q., and He, L., 2011, "Overtip Choking and Its Implications on Turbine Blade-Tip Aerodynamic Performance," J. Propul. Power, **27**(5), pp. 1008–1014.
[21] Li, W., Jiang, H., Zhang, Q., and Lee, S. W., 2014, "Squealer Tip Leakage Flow Characteristics in Transonic Condition," ASME J. Eng. Gas Turbines Power, **136**(4), p. 042601.
[22] Wang, Z., Zhang, Q., Liu, Y., and He, L., 2015, "Impact of Cooling Injection on the Transonic Over-Tip Leakage Flow and Squealer Aerothermal Design Optimization," ASME J. Eng. Gas Turbines Power, **137**(6), p. 062603.
[23] Wheeler, A. P., and Saleh, Z., 2013, "Effect of Cooling Injection on Transonic Tip Flows," J. Propul. Power, **29**(6), pp. 1374–1381.
[24] Maffulli, R., and He, L., 2014, "Dependence of External Heat Transfer Coefficient and Aerodynamics on Wall Temperature for 3-D Turbine Blade Passage," ASME Paper No. GT2014-26763.
[25] Maffulli, R., and He, L., 2013, "Wall Temperature Effects on Heat Transfer Coefficient," ASME Paper No. GT2013-94291.
[26] Zhang, Q., and He, L., 2014, "Impact of Wall Temperature on Turbine Blade Tip Aerothermal Performance," ASME J. Eng. Gas Turbines Power, **136**(5), p. 052602.
[27] Ma, H., Zhang, Q., He, L., Wang, Z., and Wang, L., 2016, "Cooling Injection Effect on a Transonic Squealer Tip—Part 1: Experimental Heat Transfer Results and CFD Validation," ASME Paper No. GT2016-57579.
[28] Zhou, C., 2015, "Thermal Performance of Transonic Cooled Tips in a Turbine Cascade," J. Propul. Power, **31**(5), pp. 1–13.
[29] Newton, P., Lock, G., Krishnababu, S., Hodson, H., Dawes, W., Hannis, J., and Whitney, C., 2006, "Heat Transfer and Aerodynamics of Turbine Blade Tips in a Linear Cascade," ASME J. Turbomach., **128**(2), pp. 300–309.
[30] Cortelezzi, L., and Karagozian, A. R., 2001, "On the Formation of the Counter-Rotating Vortex Pair in Transverse Jets," J. Fluid Mech., **446**, pp. 347–373.
[31] Smith, S. H., and Mungal, M. G., 1998, "Mixing, Structure and Scaling of the Jet in Crossflow," J. Fluid Mech., **357**, pp. 83–122.
[32] Virdi, A., Zhang, Q., He, L., Li, H., and Hunsley, R., 2015, "Aerothermal Performance of Shroudless Turbine Blade Tips With Relative Casing Movement Effects," J. Propul. Power, **31**(2), pp. 527–536.